

Exoplanet Upper Atmosphere Environment Characterization

Helmut Lammer¹, Kristina G. Kislyakova^{2,3},
Petra Odert³, Martin Leitzinger³, Maxim L. Khodachenko¹,
Mats Holmström⁴, Arnold Hanslmeier³

¹Austrian Academy of Sciences, Space Research Institute
Schmidlstr. 6, A-8042, Graz, Austria

email: helmut.lammer@oeaw.ac.at, maxim.khodachenko@oeaw.ac.at

²N.I. Lobachevsky State University, University of Nizhnij Novgorod,
23 Prospekt Gagarina, 603950 Nizhnij Novgorod, Russian Federation

email: kislyakova.kristina@gmail.com

³Institute for Physics/IGAM, University of Graz, Universitätsplatz 5, 8010 Graz, Austria
email: petra.odert@uni-graz.at, martin.leitzinger@uni-graz.at,

arnold.hanslmeier@uni-graz.at

⁴Swedish Institute of Space Physics, Box 812, SE-98128 Kiruna, Sweden
email: matsh@irf.se

Abstract. The intense stellar SXR and EUV radiation exposure at “Hot Jupiters” causes profound responses to their upper atmosphere structures. Thermospheric temperatures can reach several thousands of Kelvins, which result in dissociation of H₂ to H and ionization of H to H⁺. Depending on the density and orbit location of the exoplanet, as a result of these high temperatures the thermosphere expands dynamically up to the Roche lobe, so that geometric blow-off with large mass loss rates and intense interaction with the stellar wind plasma can occur. UV transit observations together with advanced numerical models can be used to gain knowledge on stellar plasma and the planet’s magnetic properties, as well as the upper atmosphere.

Keywords. Exoplanets, Roche lobe, mass loss, characterization, ENAs, magnetospheres

1. Introduction

Exoplanetology is one of the fastest growing fields in present-day space science. Sixteen years after the discovery of 51 Peg b, more than 550 exoplanets (August 2011) have been detected. The discovery of Jupiter-type planets at orbital distances $d < 0.05$ AU soon opened questions regarding atmospheric mass loss. In early studies of close-in exoplanets, the radiative effective temperature T_{eff} was used to estimate evaporation rates (Guillot *et al.* 1996; Konaki *et al.* 2003). In reality, the exobase temperature T_{exo} , which results from the absorption of the stellar SXR and EUV (XUV) radiation in the upper atmosphere controls thermal escape and is \gg than T_{eff} . To estimate T_{exo} of “Hot Jupiters”, Lammer *et al.* (2003) applied a scaling law which is based on an approximate solution of the heat balance equation in the thermosphere and found that the upper atmosphere of “Hot Jupiters” will be heated to several thousands of Kelvins so that hydrostatic conditions are not anymore valid.

In this work, we discuss relevant physical processes and modeling techniques, which can be used together with present and future high resolution UV observations for characterizing the upper atmosphere structure, the magnetic field, and the stellar plasma environment around close-in exoplanets. Because HD 209458b is a well-studied and

well-observed gas giant, we focus our discussions on that particular planet. In Sect. 2, we discuss the upper atmosphere structure of HD 209458b obtained from hydrodynamic and empirical models. In Sect. 3, we investigate the mass loss of H-rich hot gas giants. In Sect. 4, we discuss how one can infer knowledge related to the stellar wind plasma and magnetic properties around exoplanets from UV observations and advanced modeling techniques. In Sect. 5, we give a brief outlook to the future of such observations and studies.

2. Upper atmosphere structure of H-rich “Hot Jupiters”

2.1. Hydrodynamic models

HD 209458b is a hot gas giant with a visual radius $R_{\text{pl}} = 1.38R_{\text{Jup}}$ (Southworth 2010) and a mass $M_{\text{pl}} = 0.64 \pm 0.09M_{\text{Jup}}$ (Snellen *et al.* 2010) which orbits a ~ 4 Gyr old solar like G-type star at 0.047 AU. After the discovery of HD 209458b, several hydrodynamic models were applied to investigate the response of the stellar XUV radiation to the planet’s thermosphere (Yelle 2004, 2006; Tian *et al.* 2005; García Muñoz 2007; Penz *et al.* 2008; Murray-Clay *et al.* 2009; Guo 2011). These models solved the set of the 1D hydrodynamic fluid equations for mass, momentum and energy conservation

$$\frac{\partial n}{\partial t} + \frac{1}{r^2} \frac{\partial nvr^2}{\partial r} = 0, \quad (2.1)$$

$$n \frac{\partial v}{\partial t} + nv \frac{\partial v}{\partial r} + \frac{1}{m} \frac{\partial p}{\partial r} = n \left[-\frac{GM_{\text{pl}}}{r^2} + \frac{GM_*}{(d-r)^2} + \frac{G(M_* - M_{\text{pl}})}{d^3} (s-r) \right], \quad (2.2)$$

$$nm \left(\frac{\partial E}{\partial t} + v \frac{\partial E}{\partial r} \right) = q - p \frac{1}{r^2} \frac{\partial r^2 v}{\partial r} + \frac{1}{r^2} \frac{\partial}{\partial r} \left(r^2 \chi \frac{\partial T}{\partial r} \right), \quad (2.3)$$

with particle number density n , gas velocity v , mass m of atomic H, temperature T , Boltzmann constant k , XUV volume heating rate q , thermal pressure $p = nkT$, total energy density $E = p/[nm(\gamma-1)]$, heat conductance χ , and adiabatic index γ . Roche lobe effects due to tidal interaction as shown in Eq. (2.2) were included in García Muñoz (2007) and Penz *et al.* (2008), where G is the gravitational constant, M_{pl} the planet’s mass, M_* the host star’s mass, d is the orbital distance, and s the distance of the center of mass to the center of the planet. By solving these equations, one obtains the velocity, density and temperature profiles of the dynamically expanding and outward flowing bulk atmosphere. Yelle (2004) was the first to apply a photochemical model to HD 209458b within his 1D hydrodynamic code up to $3.3 R_{\text{pl}}$. The second hydrodynamic model, which included photochemical and ionization processes and for the first time also Roche lobe effects, was applied by García Muñoz (2007). Both model simulations indicate that the majority of the XUV radiation is absorbed or deposited between 1.05 – $1.5R_{\text{pl}}$. The hydrodynamic models of Tian *et al.* (2005) and Penz *et al.* (2008) do not include photochemistry, but use an energy deposition function as modeled by Yelle (2004) or García Muñoz (2007).

The modeled neutral H atom density in the simulation of Yelle (2004) between 2 – $3.3R_{\text{pl}}$ is $\sim 7 \times 10^{12}$ – 10^{12} m^{-3} . The temperature at the altitude range is $\sim 1.2 \times 10^4 \text{ K}$. At larger distances the temperature becomes lower due to expansion and adiabatical cooling. The outflow velocity of the bulk H atoms at $3R_{\text{pl}}$ is $\leq 2.5 \text{ km s}^{-1}$ and the mass loss rate for atomic H in the model by Yelle (2004) is $\sim 4.7 \times 10^{10} \text{ g s}^{-1}$.

Tian *et al.* (2005) applied a 1D time-dependent hydrodynamic model together with a 2D energy deposition model to HD 209458b where the inner boundary is the visual planetary radius $1R_{\text{pl}}$ and the upper boundary is $10R_{\text{pl}}$. This choice makes the Yelle model more realistic compared to Tian *et al.* (2005) because extending the hydrodynamic

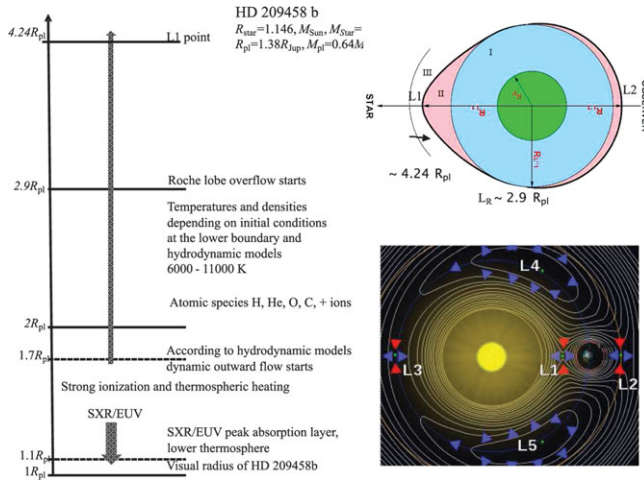


Figure 1. Left: Illustration of the upper atmosphere structure of HD 209458b or similar “Hot Jupiters” according to hydrodynamic and empirical models (Yelle 2004; Garzia Muñoz 2007; Penz *et al.* 2008; Koskinen *et al.* 2010). Right: The Roche lobe plays an important role in the mass loss of close-in exoplanets. If the XUV-heated and expanded thermosphere reaches the first Roche equipotential surface geometric blow-off occurs.

model to distances where collisions become negligible is questionable, even for the purpose of calculating the escape rate. The neutral H atom density in the model simulation of Tian *et al.* (2005) between 2–3.3 R_{pl} , depending on the assumed heating efficiency η , is about 10^{13} – 10^{12} m^{-3} . The temperature at this altitude range is $\sim 10^4$ – 3×10^4 K. The outflow velocity of the bulk H atoms at 3 R_{pl} is ~ 10 km s^{-1} . The maximum mass loss rate for H atoms in their model runs is $\sim 6 \times 10^{10}$ g s^{-1} .

García Muñoz (2007) assumed slightly different input parameters in the lower atmosphere close to 1 R_{pl} compared to Yelle (2004) and Tian *et al.* (2005), the temperature was 1200 K instead of 750 K. The upper boundary was as in Tian *et al.* (2005) at large distances $\sim 15R_{\text{pl}}$. As pointed out in Yelle (2004), such large distances may most likely not give accurate results. The H gas bulk flow velocities and number densities at $\sim 3R_{\text{pl}}$ depending on the uncertainties in the assumed initial conditions are between 5–10 km s^{-1} and 10^{13} – 10^{14} m^{-3} . This model yields temperatures $< 10^4$ K at about 3 R_{pl} comparable to Yelle (2004) and Tian *et al.* (2005). Depending on the heating efficiency and XUV flux chosen, this author obtains a loss rate of 6×10^{10} g s^{-1} .

Penz *et al.* (2008) applied a hydrodynamic model to HD 209458b by using the calculated XUV energy deposition rates of Yelle (2004) which are also in agreement with García Muñoz (2007), and obtained temperatures and mass loss rates for heating efficiencies between 20–30 % at 2–3 R_{pl} between 6000–8000 K and 1.5 – 2.5×10^{10} g s^{-1} , respectively. A temperature of $\sim 10^4$ K is obtained for a heating efficiency of 60% at an altitude range of ~ 1.5 – $1.8 R_{\text{pl}}$. After this distance, the temperature decreases due to adiabatic expansion and the non-availability of heating sources. The velocities of the outward flowing H atoms in this model are < 10 km s^{-1} at 3 R_{pl} and the density at 3 R_{pl} is $\sim 4 \times 10^{13}$ m^{-3} .

From these hydrodynamical and photochemical model simulations, we conclude that the upper atmosphere of HD 209458b and similar “Hot Jupiters” is structured as illustrated in Fig. 1. The stellar XUV radiation is absorbed mainly in the lower thermosphere $\leq 1.5R_{\text{pl}}$, where strong ionization, dissociation and heating take place. According to all hydrodynamic models discussed above, the atomic H gas at altitude levels between ~ 1.5 –

$1.7R_{\text{pl}}$ starts moving slowly and then expands dynamically upwards at a higher speed. Above $\sim 1.7\text{--}2R_{\text{pl}}$, H_2 is mainly dissociated and a huge part of the outflowing gas becomes ionized (Koskinen *et al.* 2010; Guo 2011). Depending on the boundary conditions, η and hydrodynamical models applied, the temperatures of the outward flowing H atoms between $2R_{\text{pl}}$ and the first Roche equipotential surface are about 6000–11000 K. According to these models, the present mass loss rate of HD 209458b is within a range of $\sim 10^{10}\text{--}5 \times 10^{10} \text{ g s}^{-1}$.

2.2. Empirical model results according to UV transit observations

Recently, Koskinen *et al.* (2010) developed an empirical model for the thermosphere of HD 209458b to analyze the observed HI and OI transit depths summarized by Ben-Jaffel and Hosseini (2010). Because the model atmospheres based on hydrodynamics and photochemistry are complicated and time-consuming, the empirical model applied by Koskinen *et al.* (2010) is only based on a few free parameters that can be constrained by observations and the generic features of the more complex models. The lower boundary condition is chosen at a distance of $1.1R_{\text{pl}}$. The reason for this value is also in agreement with the previously discussed hydrodynamic models that most of the XUV radiation is absorbed above $0.1 \mu\text{bar}$ and the peak absorption of the radiation occurs at a distance between $\sim 1.1\text{--}1.5R_{\text{pl}}$.

At higher altitudes, in agreement with Yelle (2004) and García Muñoz (2007), mainly H atoms populate the upper thermosphere. The atmosphere below is opaque to FUV radiation which results in a temperature of $\sim 1300 \text{ K}$. The ionization of the H atoms and other species occurs between $2R_{\text{pl}}\text{--}5R_{\text{pl}}$, this is also in agreement with the photochemical models which include ion-chemistry. According to the pressure level in Koskinen *et al.* (2010), the bulk flow velocities of the H atoms at $3R_{\text{pl}}$ are between $1\text{--}10 \text{ km s}^{-1}$, which is also in agreement with the model results of Yelle (2004), García Muñoz (2007) and Penz *et al.* (2008). According to Koskinen *et al.* (2010), two of their case studies can reproduce the HI and OI Hubble Space Telescope (HST) observations of HD 209458b best if they adopt a temperature at $2.9R_{\text{pl}}$ of 11000 K or 8000 K at $2.72R_{\text{pl}}$. The density of the H atoms at the first Roche lobe equipotential distance for 11000 K is $\sim 2.6 \times 10^{13} \text{ m}^{-3}$ and, for the cooler temperature case of 8000 K, the number density is $\sim 3.1 \times 10^{13} \text{ m}^{-3}$. According to Koskinen *et al.* (2010), the recent non-detection of auroral and dayglow emissions of H_2 from HD209458b (France *et al.* 2010) can be seen as an additional constraint and that the H_2/H dissociation front is deeper than the $0.1 \mu\text{bar}$ level. In that case, an upper atmosphere $T \sim 8000 \text{ K}$ yields the best-fitting model.

From the hydrodynamical and empirical models discussed in the previous sections, we can summarize that the upper atmosphere H atom number density n_{H} , and temperature T_{H} at $\sim 2.9R_{\text{pl}}$ of HD 209458b are most likely $\sim 3 \times 10^{13} \text{ m}^{-3}$ and $\sim 8000\text{--}10000 \text{ K}$, respectively.

3. Mass loss and the relevance of the Roche lobe

The importance of tidal forces for close-in exoplanets was first discussed by Lecavelier des Etangs *et al.* (2004). Erkaev *et al.* (2007) found that the critical temperature calculated for the modified potential barrier approaches zero when the exobase expands to the Roche lobe boundary from below, which indicates that the effect of the Roche lobe can enhance the possibility that “Hot Jupiters” may reach blow-off conditions more easily compared to similar planets in orbit locations where Roche lobe effects are negligible. It was also shown by Erkaev *et al.* (2007) that hydrodynamically modeled mass loss rates can be well approximated by a modified “energy-limited” mass loss formula

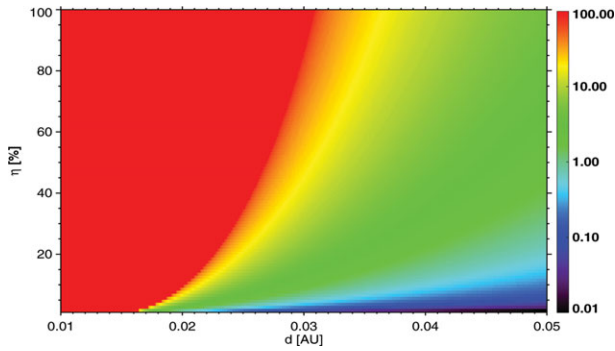


Figure 2. Mass loss of HD 209458b in planetary mass modeled over the host stars lifetime of 4 Gyr in percentage of the planets present mass as a function of orbital distance d and heating efficiency η . The XUV evolution with time of the solar-like G-type star HD 209458 is taken from the power law given in Ribas *et al.* (2005).

$dM/dt = [3\eta F_{\text{XUV}}(t)]/[4G\rho_{\text{pl}}K(\xi)]$, which includes a mass loss enhancement factor $K(\xi)$ which depends non-linearly on a dimensionless Roche lobe boundary distance $\xi = R_{\text{L}}/R_{\text{pl}}$ (Erkaev *et al.* 2007) and realistic $\eta \ll 100\%$ (Lammer, *et al.* 2009) for the stellar XUV radiation. $F_{\text{XUV}}(t)$ is the XUV flux corresponding to the stellar age at the orbital distance of the planet, ρ_{pl} is the planetary density and G Newton's gravitational constant.

Fig. 2 shows the modeled mass loss of HD 209458b over the host star's lifetime of 4 Gyr in percentage of the planetary mass at various orbital locations and values of η . One can see that the mass loss is highly overestimated if one applies the energy-limited approach with $\eta = 100\%$. In reality, the ratio of the net heating rate to the rate of stellar energy absorption is $\sim 15\text{--}20\%$ (e.g., Lammer *et al.* 2009; Murray-Clay *et al.* 2009). At HD 209458b's orbit location of 0.047 AU, the planet lost a negligible fraction of its mass. If a planet with the same initial density would be at $d < 0.025$ AU, such a planet may shrink to an Uranus-type body or even evaporate to its core mass due to the Roche lobe effect. Depending on a stellar spectral type of the host star, planetary density, η , d , and the related Roche lobe effect, we expect that at distances between 0.01–0.025 AU Jupiter-class and sub-Jupiter-class exoplanets can lose several percent of their initial masses and planets which originated with low densities may even evaporate down to their cores.

4. Characterization of the upper atmosphere-magnetosphere environment by UV observations and advanced numerical models

HST observations during transits of HD 209458b in the UV show absorption in the stellar Lyman- α line at 1215.67Å. Vidal-Madjar *et al.* (2003) used the G140M grating during the observation of 3 transits with a spectral resolution of $\sim 0.08\text{Å}$, which allowed a detailed analysis of the line profile of the H Lyman- α emission line, where they obtained a transit depth of $15 \pm 4\%$ from the ratio of the fluxes in two wavelength (λ) regions around the core of the H Lyman- α line to the flux in the wings of the line during transit. After the observation and data interpretation of Vidal-Madjar *et al.* (2003) and several debates regarding the analysis of these observations, two subsequent observations with lower spectral resolution with the HST STIS/ACS instruments (Ehrenreich *et al.* 2008; Vidal-Madjar *et al.* 2008) were carried out and convinced now also sceptics that the transit depth in the stellar Lyman- α line is significantly greater than the transit depths expected from the planetary disk alone (Vidal-Madjar *et al.* 2008; Ben-Jaffel and Sona Hosseini 2010). Besides these Lyman- α observations, additional transits of HD 209458b

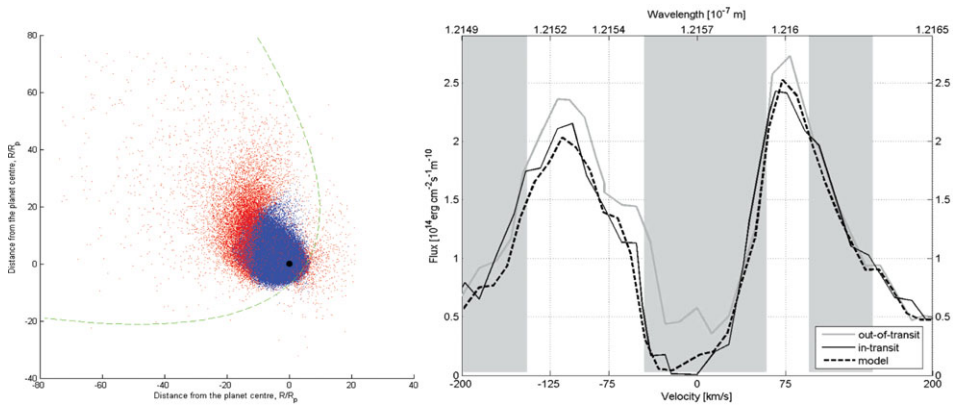


Figure 3. Left: Modeled stellar wind interaction with HD 209458b with an assumed magnetopause (dashed green line) sub-stellar obstacle at $\sim 4.7R_{p1}$. Shown from above, perpendicular to HD 20948b's orbital plane as seen from Earth, along the direction of the x-axis. The stellar wind protons are not plotted but flow around the magnetopause obstacle and interact with the planetary hydrogen exosphere (blue dots) and produce energetic neutral atoms (ENAs: red dots). Right: Modeled attenuation spectra and comparison with the HST/STIS observations of Vidal-Madjar *et al.* (2003). Observed profile before transit (bold line); observed profile during transit (thinner line). The dashed line is the modeled profile which is computed at the instant of mid-transit for stellar wind density and velocities $n_{sw} \approx 2.5\text{--}3.5 \times 10^9 \text{ m}^{-3}$ and $100 \text{ km s}^{-1} < v_{sw} < 250 \text{ km s}^{-1}$ and a sub-stellar stand-off distance $R_s \approx 4.5R_{p1}$.

were observed with the HST/STIS and COS spectrographs in the λ range 1180–1710 Å and indicated absorptions of O, C and Si multiply charged ions (Vidal-Madjar *et al.* 2004; Linsky *et al.* 2010).

There are three important points which should also be mentioned related to UV observations and the empirical model described in Sect. 2 of Koskinen *et al.* (2010). First, the upper atmosphere temperatures between 8000–10000 K are based on the assumption that the observed O, C and Si particles are of planetary origin, so that they are dragged upward by the planetary H wind. One should note that the upper atmosphere temperature could be ≤ 8000 K if these particles originate within the stellar wind plasma, as now expected for Mg ions around WASP-12b (Llama *et al.* 2011). Second, Koskinen *et al.* (2010) fitted their model to the transit depth measurements covering the full width of the stellar H Lyman- α profile in the λ range 1212–1220 Å with absorption depths of $6.6 \pm 2.3\%$ (Ben-Jaffel and Hosseini 2010) and not to the early Vidal-Madjar *et al.* (2003) observations. One should note that the empirical model atmospheres can more easily fit the lower absorption depths without introducing an external H source. Third, large column densities along the lines-of-sight through the atmosphere are necessary, which depend on the pressure level of the model-dependent H₂/H dissociation levels. For explaining the high velocity H atoms in the flanks of the HST attenuation spectra, Koskinen *et al.* (2010) argue that, due to natural and thermal broadening and large column densities along the lines-of-sight through the atmosphere, the optical depth in the wings of the line profile can be significant even in the absence of actual bulk flows towards or away from the observer.

However, this interpretation gets into trouble due to another observation of an extended upper atmosphere by Lyman- α absorption during transits of HD 189733b (Lecavelier des Etangs *et al.* 2010). Guo (2011) studied the upper atmosphere structure of HD 189733b, which is exposed to a higher XUV flux, and found that in contrast to HD 209458b, $\sim 80\%$ of its dynamically expanding upper atmosphere is ionized so that its planetary

wind is almost composed of H^+ ions. Under this circumstance, the remaining neutral bulk atmosphere cannot produce the detected adequate absorption in Lyman- α . Because of the steep decline of the number density of neutral H atoms, the optical depth in the wing of the line is very low. If the amount of atomic H is not adequate to fit the observations, the fact that the transits of HD 189733b in H Lyman- α have been observed imply that external processes, such as the production of energetic neutral atoms (ENAs) as suggested by Holmström *et al.* (2008) and Ekenbäck *et al.* (2010), play an important role. One should also note that even in case the assumption of Koskinen *et al.* (2010) is right, ENAs will be produced if the upper atmosphere interacts with the stellar wind plasma. This agrees with another finding of Koskinen *et al.* (2010) that the upper boundary of their model is close to both the boundary of the Roche lobe and an ionopause of a weakly magnetized planet and that the density of the outward flowing neutral atoms decreases sharply above this boundary. If this is the case, the production of ENAs in the Lyman- α attenuation spectra cannot be neglected. Shematovich (2010) studied the production and escape of dissociated hot H atoms from HD 209458b, which have velocities $< 45 \text{ km s}^{-1}$ with the majority of the atoms at $\sim 20 \text{ km s}^{-1}$. Thus, it is difficult that thermal and non-thermal planetary atoms reach velocities $\geq 100 \text{ km s}^{-1}$ which were observed in the high energy part of the spectrum.

ENAs will be produced by charge exchange with stellar wind protons and neutral H atoms from the planetary upper atmosphere. In Fig. 3, we show two modeled hydrogen corona and ENAs as well as the attenuation spectra in comparison with the HST/STIS in and out of transit observations of Vidal-Madjar *et al.* (2003). We apply the same plasma flow, exosphere, ENA production and Lyman- α attenuation model described in detail in Holmström *et al.* (2008) and Ekenbäck *et al.* (2010) to the planetary parameters favored by Koskinen *et al.* (2010). The results shown in Fig. 3 indicate that the sub-stellar magnetopause obstacle should be located between $4.5\text{--}6R_{\text{pl}}$ corresponding to a magnetic moment of $\approx 40\%$ that of Jupiter's.

5. Future outlook

Our studies show that future high resolution UV observations of exoplanets by space observatories like the Russia-led World Space Observatory-UV (WSO-UV) in combination with discovered transiting exoplanets around “bright” stars as planned with ESA's PLATO mission would open a promising field for the characterization of the stellar plasma environment and its interaction with exoplanet upper atmospheres and magnetospheres. From these observations, we would obtain knowledge on the stellar wind and magnetic properties of the exoplanet as well as its upper atmosphere structure and mass loss.

Acknowledgements

H. L., K. G. K., M. H., and M. L. K. acknowledge the ISSI team “Characterizing stellar- and exoplanetary environments.” H. L., K. G. K. & M. L. K. thank the RFBR-FWF project 09-02-91002-ANF_a / I199-N16, the FWF project P21197-N16. A.H, P. O. and M. L. acknowledge the FWF project P22950-N16. K. G. K. also acknowledge the RFBR project 08-02-00119_a, the NK-21P and the Russian Education Ministry. The authors also thank the EU FP7 project IMPEX (No.262863) and the EUROPLANET-RI projects, JRA3/EMDAF and the Na2 science WG4 and WG5 for support.

References

- Ben-Jaffel, L. & Hosseini, Sona, S. 2010, *ApJ*, 709, 1284
- Ekenbäck, A., Holmström, M., Wurz, P., Grießmeier, J.-M., Lammer, H., Selsis, F., & Penz, T. 2010, *ApJ*, 709, 670
- Ehrenreich, D., Lecavelier des Etangs, A., Hébrard, G., Désert, J.-M., Vidal-Madjar, A., McConnell, J. C., Parkinson, C. D., Ballester, G. E., & Ferlet, R. 2008, *A&A*, 483, 933
- Erkaev, N. V., Kulikov, Yu. N., Lammer, H., Selsis, F., Langmayr, D., Jaritz, G. F., & Biernat, H. K. 2005, *A&A*, 472, 329
- France, K., Stocke, J. T., Yang, H., Linsky, J. L., Wolven, B. C., Froning, C. S., Green, J. C., & Osterman, S. N. 2010, *ApJ*, 712, 1277
- García Muñoz, A. 2007, *Planet. Space Sci.*, 55, 1426
- Guillot, T., Burrows, A., Hubbard, W. B., Lunine, J. I., & Saumon, D. 1996, *ApJ*, 459, L35
- Guo, J. H. 2011, *ApJ*, 733, 98
- Holmström, M., Ekenbäck, A., Selsis, F., Penz, T., Lammer, H., & Wurz, P. 2008, *Nature*, 451, 970
- Konacki, M., Torres, G., Jha, S., & Sasselov, D. 2003, *Nature*, 421, 507
- Koskinen, T. T., Yelle, R., Lavvas, P., & Lewis, N. K. 2010, *ApJ*, 723, 116
- Lammer, H., Selsis, F., Ribas, I., Guinan, E. F., & Bauer, S. J. 2003, *ApJL*, 598, L121
- Lammer, H., Odert, P., Leitzinger, M., Khodachenko, M. L., Panchenko, M., Kulikov, Yu. N., Zhang, T. L., Lichtenegger, H. I. M., Erkaev, N. V., Wuchterl, G., Micela, G., Penz, T., Biernat, H. K., Weingrill, J., Steller, M., Ottacher, H., Hasiba, J., & Hanslmeier, A. 2009, *A&A*, 506, 399
- Lecavelier Des Etangs, A., Vidal-Madjar, A., McConnell, J. C., & Hébrard, G. 2004, *A&A*, 418, L1
- Lecavelier Des Etangs, A., Ehrenreich, D., Vidal-Madjar, A., Ballester, G. E., Désert, J.-M., Ferlet, R., Hébrard, G., Sing, D. K., Tchakoumegni, K.-O., & Udry, S. 2010, *A&A*, 514, A72
- Linsky, J. L., Yang, H., France, K., Froning, C. S., Green, J. C., Stocke, J. T., & Osterman, S. N. 2010, *ApJ*, 717, 1291
- Llama, J., Wood, K., Jardine, M., Vidotto, A. A., Helling, Ch., Fossati, L., & Haswell, C. A. 2011, *MNRAS*, in press
- Murray-Clay, R. A., Chiang, E. I., & Murray, N. 2009, *ApJ*, 693, 23
- Penz, T., Erkaev, N. V., Kulikov, Yu. N., Langmayr, D., Lammer, H., Micela, G., Cecchi-Pestellini, C., Biernat, H. K., Selsis, F., Barge, P., Deleuil, M., & Léger, A. 2008, *Planet. Space Sci.*, 56, 1260
- Shematovich, V. I. 2010, *Solar Sys. Res.*, 44, 96
- Snellen, I. A. G., de Kok, R. J., de Mooij, E. J. W., & Albrecht, S. 2010, *Nature*, 465, 1049
- Southworth, J. 2010, *MNRAS*, 408, 1689
- Tian, F., Toon, O. B., Pavlov, A. A., & Sterck, H. D.e. 2005, *ApJ*, 621, 1049
- Vidal-Madjar, A., Lecavelier Des Etangs, A., Désert, J. M., Ballester, G. E., Ferlet, R., Hébrard, G., & Mayor, M. 2003, *Nature*, 422, 143
- Vidal-Madjar, A., Désert, J.-M., Lecavelier Des Etangs, A., Hébrard, G., Ballester, G. E., Ehrenreich, D., Ferlet, R., McConnell, J. C., Mayor, M., & Parkinson, C. D. 2004, *ApJ*, 604, L69
- Vidal-Madjar, A., Lecavelier Des Etangs, A., Désert, J.-M., Ballester, G. E., Ferlet, R., Hébrard, G., & Mayor M. 2008, *ApJ*, 676, 57
- Yelle, R. V. 2004, *Icarus*, 170, 167

Discussion

A. TRIAUD: Do you include in the calculations for mass loss the fact that orbits delay? This is the idea is that “Hot Jupiters” might have circularized from longer period eccentric orbits.

H. LAMMER: This was not taken into account. The difference in the results are smaller relative to the mass loss if one compares it to the uncertainties in the XUV flux or heating efficiencies.